

Geochemistry, Geophysics, Geosystems®



RESEARCH ARTICLE

10.1029/2021GC009995

Key Points:

- Shifts in pearl nacre Raman data that align with $\delta^{18}\text{O}_{\text{Arg}}$ and seasonal lake environmental conditions may lead to future mineralogy-based proxies
- SIMS-based $\delta^{18}\text{O}_{\text{Arg}}$ correlate with relative nacre OH/O as well as lake temperature, dissolved oxygen, and light levels at 1 m depth
- Nacre tablet thickness correlates with relative nacre OH/O and electrical conductivity in Kentucky Lake, but not with seasonal temperatures

Supporting Information:

Supporting Information may be found in the online version of this article.

Correspondence to:

G. A. Farfan,
farfang@si.edu

Citation:

Farfan, G. A., Zhou, C., Valley, J. W., & Orland, I. J. (2021). Coupling mineralogy and oxygen isotopes to seasonal environmental shifts recorded in modern freshwater pearl nacre from Kentucky Lake. *Geochemistry, Geophysics, Geosystems*, 22, e2021GC009995. <https://doi.org/10.1029/2021GC009995>

Received 22 JUN 2021

Accepted 15 NOV 2021

Author Contributions:

Conceptualization: G. A. Farfan, C. Zhou, J. W. Valley

Data curation: G. A. Farfan

Formal analysis: G. A. Farfan, I. J. Orland

Funding acquisition: C. Zhou

Investigation: G. A. Farfan, C. Zhou, J. W. Valley, I. J. Orland

Methodology: G. A. Farfan, C. Zhou, J. W. Valley, I. J. Orland




Project Administration: G. A. Farfan

Resources: C. Zhou, J. W. Valley

© 2021 Smithsonian Institution.

This is an open access article under the terms of the [Creative Commons Attribution-NonCommercial-NoDerivs License](https://creativecommons.org/licenses/by/4.0/), which permits use and distribution in any medium, provided the original work is properly cited, the use is non-commercial and no modifications or adaptations are made.

Coupling Mineralogy and Oxygen Isotopes to Seasonal Environmental Shifts Recorded in Modern Freshwater Pearl Nacre From Kentucky Lake

G. A. Farfan¹ , C. Zhou², J. W. Valley³ , and I. J. Orland^{3,4} 

¹Smithsonian Institution, National Museum of Natural History, Washington, DC, USA, ²Gemological Institute of America, New York, NY, USA, ³Department of Geoscience, University of Wisconsin, Madison, WI, USA, ⁴Wisconsin Geological and Natural History Survey, University of Wisconsin, Madison, WI, USA

Abstract Biominerals that accrete shell or skeleton are commonly used as windows to past geochemical environments. Using biominerals as paleoproxies depends on the assumption that biominerals faithfully and predictably record environmental parameters, yet little has been done from a mineralogical perspective to understand how various environmental shifts impact shell and skeleton mineralogy and how mineralogy influences proxy calibrations. In this study, we correlate a suite of environmental data from the Kentucky Lake Long-Term Monitoring Program with mineralogical and chemical signatures of modern cultured pearl nacre. Six transects were measured across three pearls from nucleus to edge for oxygen isotope ratio ($\delta^{18}\text{O}$) using SIMS (10- μm spots) and for mineralogy via nacre tablet thickness using SEM and via carbonate bonding environments using Raman spectroscopy. After confirming a strong seasonal correlation between $\delta^{18}\text{O}$ and temperature, we extend $\delta^{18}\text{O}$ correlations to relative nacre OH/O ratios, lake dissolved oxygen, and lake light levels at 1 m depth. Although nacre tablet thicknesses are not clearly correlated with temperature, we observe correlative trends with lake conductivity and relative nacre OH/O ratios. For the Raman spectroscopy measurements, there was a modest inverse correlation between increasing carbonate ν_1 and ν_4 vibrational mode peak heights with $\delta^{18}\text{O}$ and lake dissolved oxygen levels. Standard deviations in Raman T:L peak area ratios, as an estimation of angle spread of tablet crystallographic orientation, correlate with lake reduction potential. This approach of combining geochemical, isotopic, mineralogical, and environmental data lends a more holistic view to biomineralization in natural systems and to the decoding of environmental mineral signatures.

Plain Language Summary For over a century, humans have been mastering mollusk farming techniques to grow pearls for ornamental purposes. Like tree rings, these cultured pearls grow in concentric layers over time. We can slice these pearls in half to use them as pristine time capsules that reveal the past local environmental conditions in which they grew. In this study, we show how seasonal temperature, dissolved oxygen, electrical conductivity, and other environmental parameters in Kentucky Lake, KY are reflected as mineral and chemical shifts in the pearl mineral layers as they grew over several years. For the first time, we combine high spatial-resolution chemical signals (oxygen isotopes) with detailed corresponding mineralogical textures and atomic-scale crystal structure information to find that mineralogy holds the potential to independently trace environmental signals within pearls. This has implications for using similar low-cost, mineral-based methods to trace paleoenvironments in fossil pearls and shells, and for predicting the impact of future environmental shifts on pearl quality.

1. Introduction

From rising temperatures, to shifting carbonate chemistry, to extreme storms, modern calcifying organisms experience many environmental stressors as they build their shells and skeletons in the face of climate change and other anthropogenic influences. Nacre-forming mollusks present in both saltwater and freshwater environments are economically important as food and as drivers of the pearl industry. Thus, understanding how nacre is impacted by seasonal and long-term environmental shifts is essential to assessing the health of this resource across the globe. As they grow, nacre and other biomineralizing carbonates are thought to record their local growth environments in their crystallography and chemistry, an assumption that has been successfully applied for paleoproxies in estimating past environments over geologic time. Understanding seasonal variations in both the mineralogy and isotope ratios of modern biocarbonate systems may help to better inform these paleoproxies and determine

Software: I. J. Orland
Supervision: J. W. Valley
Validation: J. W. Valley, I. J. Orland
Visualization: G. A. Farfan
Writing – original draft: G. A. Farfan
Writing – review & editing: G. A. Farfan, C. Zhou, J. W. Valley, I. J. Orland

which environmental conditions hold the greatest influence over biocarbonate mineralogical and chemical signatures. In this case study, we focus our efforts on modern freshwater mollusk nacre in the form of farmed cultured pearls that are accompanied by extensive, high-resolution environmental records of nearby Kentucky Lake, KY, USA. This study is one of the first to apply both detailed mineralogical data and high-resolution SIMS-based $\delta^{18}\text{O}$ data to perform paleoproxy work on pearl nacre.

1.1. Oxygen Isotope Ratios in Mollusks as a Classic Temperature Proxy

Oxygen isotope ratios ($\delta^{18}\text{O}$) are extensively used as a proxy to trace seasonal and long-term temperature fluctuations recorded in an array of biocarbonates, ranging from modern to ancient and seawater to freshwater, including foraminifera (Pearson, 2012; Spero et al., 1997), corals (Weber & Woodhead, 1972), otoliths (Helser et al., 2018; Høie et al., 2004; Kalish, 1991), and mollusks (Dettman et al., 1999). Mollusks are particularly well-known tracers of past environments since they are ubiquitous and their oxygen isotopes have been studied in marine (e.g., Freitas et al., 2005; Gibson et al., 2001; Leng & Lewis, 2016; Linzmeier et al., 2018), freshwater (e.g., Dettman et al., 1999; Fritz & Poplawski, 1974), and terrestrial (e.g., Abell, 1985) environments. Mollusk nacre is also an ideal model system to study environmental signals in bioaragonite because the mineralogy, morphological structure, and formation mechanisms of mollusk nacre have been widely studied from biological and materials perspectives (e.g., Addadi et al., 2006; Checa, 2018; Checa et al., 2013; DeVol et al., 2015; Gim et al., 2019; Nudelman, 2015; Olson et al., 2013). In particular, nacre architecture is composed of flat tablets of aragonite interlayered with β -chitin and a silk hydrogel of acidic proteins, which gives this biomaterial composite-material properties (added strength, interesting optical properties, etc.) as the nacre grows layers over time (Addadi et al., 2006; Gim et al., 2019). Despite the strong biological influence on aragonite nacre tablet nucleation and growth, environmental factors (e.g., temperature, ocean acidification) have also been shown to directly impact nacre morphology and mollusk shell material properties (e.g., Gilbert et al., 2017; Mackenzie et al., 2014; Martínez et al., 2018). Because these biomineral environmental samples are subject to many interrelated variables (temperature, dissolved oxygen, pH, and salinity), the interpretation of oxygen isotope ratios as an environmental chemical tracer is still an active topic of research.

Freshwater mollusk nacre studies provide compelling examples of seasonal freshwater lake and stream temperature fluctuations strongly mirroring $\delta^{18}\text{O}_{\text{Arg}}$ across transects of unioid shells sampled via SIMS and micro-milling (e.g., Dettman et al., 1999; Fritz & Poplawski, 1974; Goodwin et al., 2019; Pfister et al., 2018). Transects of $\delta^{18}\text{O}_{\text{Arg}}$ in pearl nacre have also been performed at lower spatial resolution (Yoshimura et al., 2010). These studies establish that: (a) $\delta^{18}\text{O}$ signals from source water ($\delta^{18}\text{O}_{\text{water}}$) are recorded by shell aragonite ($\delta^{18}\text{O}_{\text{Arg}}$), (b) nacre growth pauses under periods of colder temperatures ($<10\text{--}12^\circ\text{C}$) in freshwater environments, and (c) $\delta^{13}\text{C}$ ratios appear to be relatively homogenous and not particularly reflective of environmental changes. To complement these $\delta^{18}\text{O}_{\text{Arg}}$ observations in natural shells, abiotic synthetic carbonate experiments have targeted how temperature (Kim et al., 2007; Zhou & Zheng, 2003), growth rate (Watkins et al., 2013), and Mg concentrations (Kim et al., 2007) each impact $\delta^{18}\text{O}$ signals. Decidedly, temperature and $\delta^{18}\text{O}$ of lake water have the strongest effect on the $\delta^{18}\text{O}_{\text{Arg}}$ signals that are recorded by the carbonates. This is the first study to perform SIMS-based $\delta^{18}\text{O}_{\text{Arg}}$ measurements to investigate records of seasonality in freshwater pearls.

1.2. The Role of Mollusk Nacre Mineralogy in Environmental Proxies

Rather than relying solely on oxygen isotopes as a paleoproxy, recent studies on nacre mineralogy (crystal morphology, structure, and chemistry) are starting to uncover relationships between crystallographic properties and environmental conditions that could serve as independent mineralogical proxies. For instance, on the nano- to micrometer-scale, nacre thickness (Gilbert et al., 2017; Olson et al., 2012; Rousseau & Rollion-Bard, 2012) and nacre tablet crystallographic orientation (Olson & Gilbert, 2012) are proposed to change as a function of surrounding seawater temperature and pressure conditions ranging from $\sim 2\text{--}30^\circ\text{C}$ and $\sim 0\text{--}600$ m depth over modern and geologic timescales. In culturing experiments, Höche et al. (2021) also observe shifts in *Arctica islandica* microstructure in the non-nacreous hinge plate region of the shell as a function of increasing temperature. Beyond changes in tablet morphology and orientation with temperature, little else has been explored to tie the micron- to atomic-scale mineralogy and crystal structures of nacre aragonite to specific shifts in surrounding environmental and growth conditions, as has been previously examined in coral aragonite (DeCarlo et al., 2017; Farfan et al., 2018). On the millimeter to micrometer scale, confocal Raman spectroscopy, Mutvei's solution technique,

and fluorescence mapping can be utilized to visualize internal growth patterns in paleontological bivalve shells for the purposes of sclerochronology and to infer seasonal environmental shifts (Beierlein et al., 2015; Linzmeier et al., 2018). These kinds of mineralogical observations could prove particularly useful in cases where high-resolution SIMS measurements are not readily available. However, it is not known how these mineralogical signatures relate to oxygen isotope signals on modern seasonal timescales and how reliable they are for tracing temperature and other environmental variables that may impact mollusk aragonite biomineralization. Recently, Trofimova et al. (2018) observed that different domains within time-equivalent shell growth have distinct oxygen isotope ratios, which raises important questions about the influence of microstructure on shell $\delta^{18}\text{O}$ and temperature proxy interpretations. Pearl nacre opens a unique opportunity, since it consists of a single kind of microstructure with an ideal geometry for measuring a compact geochemical transect with a known timeframe. These kinds of studies indicate that coupling mineralogy to isotope ratios is a promising approach for future studies of paleoreconstructions and research presented here seeks to add to this active line of research.

Beyond the paleoproxy applications, this study also has implications for gem science. Currently, pearls are found and grown all around the world, with different prices associated with pearls from specific localities. The pearl industry is particularly interested in finding ways to non-destructively test for parameters that could pinpoint the country of origin of a pearl. Understanding what controls isotopic and geochemical signals in pearls is a critical first step to creating a database of pearl provenance parameters. Beyond pearl provenance, gem science studies have also tackled how different environments (temperature, salinity, and light) impact pearl nacre quality and tablet thickness (Cahn, 1949; Gervis & Sims, 1992; Kripa et al., 2007; Rao & Rao, 1974). Most notably, these studies indicate that nacre growth rates and nacre thickness can be correlated with temperature and with chlorophyll levels as a measure of food abundance (Latchere et al., 2018; Tomaru et al., 2002). From the broader perspective of mollusk health, aquaculture studies of mollusks across the globe point to temperature as the primary stressor on shell strength and health (e.g., Mackenzie et al., 2014; Martinez et al., 2018), and in calcitic Ostreidae family shells, experimental observations reveal that weaker shells are associated with combined low salinity and high pCO_2 conditions (Dickinson et al., 2012).

In this case study, we capitalize on farmed cultured pearls as relatively pristine time capsules of a singular mineral phase and morphology with a known age to take a cross-disciplinary approach (isotopic, environmental, and gem science) to connect modern seasonal environmental shifts with $\delta^{18}\text{O}$ and mineralogical (nacre thickness and Raman-active carbonate bonding environments) proxies and trends. We hypothesize that pearls, like other biominerals, could be recorders of paleoclimate and seasonality. If this is true, then we seek to test whether pearls grown in natural environments exhibit shifts in their mineralogy (crystal morphology, atomic crystal structure, and chemistry) that match seasonal environmental patterns.

1.3. Raman Spectroscopy in Mollusk Biomineral Studies

In order to non-destructively assess the crystal structure of the nacre aragonite, we focus on Raman spectroscopy methods to probe the bonding vibrational modes of trigonal-planar carbonate groups in the aragonite unit cell (Figure 1). The dominant ν_1 vibrational mode represents the symmetric stretching of the carbonate group. The second-most dominant peaks are the lattice modes which occur below 300 cm^{-1} and represent translational and librational vibrations. The weakest peaks represent the in-plane and out-of-plane bending ν_4 and ν_2 modes, respectively. Typically, major shifts in peak positions in carbonates reflect drastic changes in vibrational mode frequency associated with extreme high pressure or temperature conditions (e.g., Biellmann & Gillet, 1992). Otherwise, shifts in peak positions or additional peaks are used as fingerprints to denote the presence of other mineral phases. Previous studies suggest that shifts in Raman peak heights in abiogenic carbonates and in a gastropod shell are signs of shifting crystallographic orientation within the shell or between crystallites (Murphy et al., 2021; Nehrke & Nouet, 2011). In particular, these studies indicate that the translation:libration (T:L) mode ratio (or 153 cm^{-1} : 206 cm^{-1} peak ratio) of peak areas (Nehrke & Nouet, 2011) and peak heights (Murphy et al., 2021) represent rotations of the *a*- and *b*- axes perpendicular to the *c*-axis (see rendition of the aragonite unit cell in Figure 1). In parallel to previous Raman observations of T:L ratios signaling crystallographic orientation, another study on nacre tablet crystallographic orientations demonstrates that increased angle spread of the relative crystalline orientation of nacre tablets (as determined by small polarization-dependent imaging contrast [PIC] maps) can be correlated with increasing temperature (Olson & Gilbert, 2012).

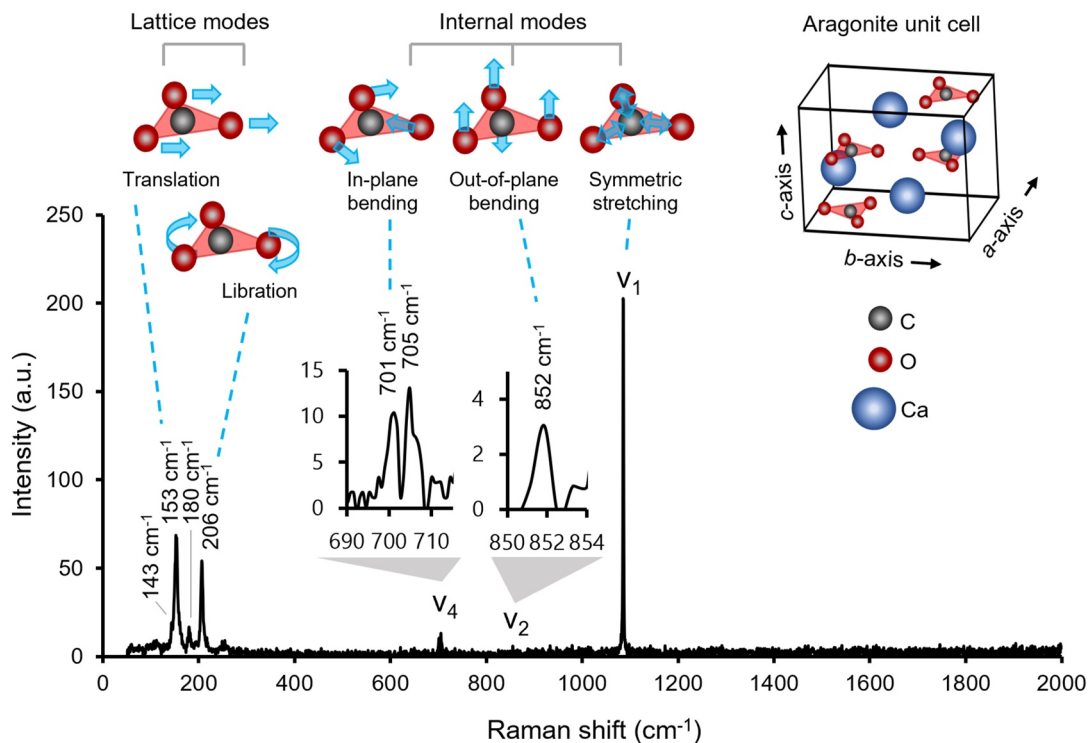


Figure 1. Representative Raman spectrum of Kentucky Lake pearl aragonite labeled with peak positions consistent with lattice and internal vibrational modes described by Urmos et al. (1991) and Bischoff et al. (1985). Approximate renditions of translational, librational, bending, and stretching vibrations of the carbonate groups are depicted above the peaks. We also include a diagram of the aragonite unit cell to demonstrate how the carbonate groups and their vibrations fit within the crystal structure.

Oxygen isotope analyses and other techniques previously used to tie environmental data to biomineral carbonate records at high spatial resolution are expensive and not always readily available. Thus, as confocal Raman spectroscopy mapping becomes more accessible across research universities and institutions, exploring how this high-resolution, non-destructive, and relatively inexpensive technique could serve as an independent mineralogical proxy is of great interest to the paleoproxy research community. Proof-of-concept mapping Raman studies on modern and fossil mollusk samples in which Raman maps were compared to more traditional staining and fluorescence mapping techniques indicate that Raman may prove a useful tool in interrogating the seasonal cycles of shell growth for archival purposes (Beierlein et al., 2015). Milano et al. (2017) stress that the multivariable nature of biomineralization and environmental settings make it difficult to untangle the effect of individual variables; however, their incubation experiments on *Arctica islandica* and subsequent Raman maps suggest that Raman-based measurements of crystallographic orientation may be applied as an independent proxy for formation temperature in that system. Here we apply this idea to a freshwater mollusk system and compare Raman spectroscopy maps with a broader suite of seasonal environmental variables, as well as to $\delta^{18}\text{O}$ and nacre tablet thickness environmental proxies, to explore which variables may be most involved in influencing modern nacre aragonite Raman vibrational modes.

2. Materials and Methods

2.1. Samples

Freshwater cultured pearls are pearls formed when mussels are inoculated with a mother-of-pearl bead and accompanying epithelial cells by a pearl farmer via a very delicate surgery. The inoculated mussel is then placed back in the lake, where it lives similarly to a wild mussel and grows pearl nacre around the bead irritant. In some cases, the epithelial cells become separated from the bead and an irregular-shaped pearl grows over the cells, known as a “keshi” pearl. The American Pearl Company farmed freshwater cultured pearls over the past several decades and this study investigates three keshi pearls (along two transects each) from Washboard mussels

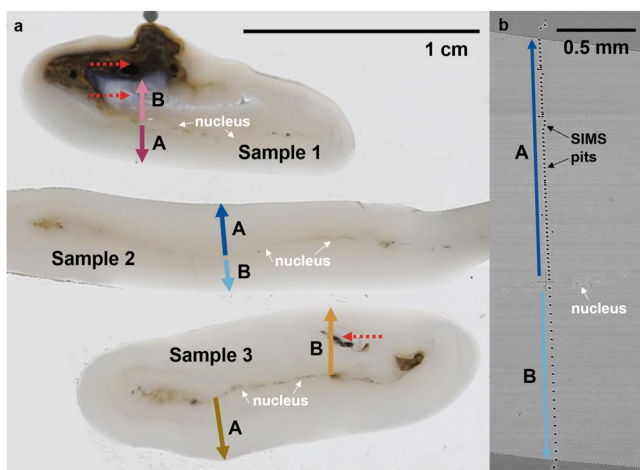


Figure 2. (a) Optical image of the three freshwater pearl samples used in this study and the positions of mirroring transects (A and B) from nucleus to exterior, along which chemical and mineralogical data were collected. Red dashed arrows highlight areas where the transects are interrupted by imperfections and debris. Organic material that formed the nucleus of the pearls are indicated by white arrows. (b) SEM micrograph of the A and B transects of 10 μm SIMS pits made across Sample 2.

(*Megalonaias nervosa*) that were harvested between 1995 and 1997 (Samples 1, 2) and 2002–2004 (Sample 3) at their pearl farms near Camden, TN, located ~ 80 km south of environmental monitoring stations in Kentucky Lake, KY, USA. The pearls at this farm were typically inoculated in the early spring, grown in the lake near Camden, TN for two to four years at <1 m depth, and harvested in late September to early October. This fall harvest season is consistent each year due to pearl nacre growth exhibiting better-quality luster as water temperatures begin to drop. The three cultured pearls in this study were cast in epoxy, ground to their midsections, polished, and gold-coated for SIMS measurements and imaging by scanning electron microscopy (SEM). The gold coating was later polished away to perform Raman spectroscopy measurements. The three pearl samples and the positions of the two transects on each sample (A and B) for which we collected isotopic and mineralogical data are pictured in Figure 2. “A” transects are selected as more pristine transects that are predominantly featured in this study; while “B” transects are mirror transects (Figure 2a). In Sample 2, both A and B transects are pristine (Figure 2b), whereas Samples 1 and 3 have B-transects that are interrupted by large debris inclusions (Figure 2a, red dashed arrows).

2.2. Secondary Ion Mass Spectrometry (SIMS)

Secondary Ion Mass Spectrometry (SIMS) was performed using a CAMECA IMS 1280 at the WiscSIMS Lab, Department of Geoscience, University of Wisconsin-Madison. Spot transects from the interior nucleus of the cultured

pearl to the outermost growth layer were performed on the three pearl samples. Replicate transects were measured on each side of the pearl and are labeled as transects “A” and “B” for all three pearls (Figure 2) with A designating the transect with fewer visible inclusions.

For each SIMS analysis, a ~ 1.1 nA $^{133}\text{Cs}^+$ primary ion beam was focused on the sample surface to sputter a ~ 10 μm diameter, ~ 1 μm -deep pit into the aragonite. Sputtered secondary ions of $^{16}\text{O}^-$, $^{16}\text{OH}^-$, and $^{18}\text{O}^-$ were accelerated into a double-focusing mass spectrometer and counted simultaneously by three Faraday cup detectors. The typical secondary ion count rate for $^{16}\text{O}^-$ was 2.2 Gcps. Each group of 10–15 sample spots was bracketed by two groups of 4–5 spot analyses each on the calcite running standard UWC-3 ($\delta^{18}\text{O} = 12.49\text{‰}$ Vienna Standard Mean Ocean Water, VSMOW; Kozdon et al., 2009).

The bracketing analyses of UWC-3 were used to calibrate data to the VSMOW scale, evaluate any possible drift and calculate the precision of intervening sample $\delta^{18}\text{O}$ analyses, with an average 2 s.d. of 0.25‰ for the entire session. UWC-3 analyses were also used to establish background $^{16}\text{OH}^-/^{16}\text{O}^-$ (OH/O hereafter) for each group of samples since the amphibolite facies calcite standard is understood to contain effectively no water; the average OH/O of bracketing standards is subtracted from the OH/O of intervening samples and reported in Table S1 of Supporting Information S1 as OH/O-corrected (Wang et al., 2014). Raw values of sample $\delta^{18}\text{O}$ were corrected to the VSMOW (and VPDB) scale by calculating the mass bias of bracketing UWC-3 measurements, then uniformly adjusting that bias to account for the difference in bias between the aragonite sample and the calcite standard. Values of $\delta^{18}\text{O}_{\text{VSMOW}}$ were converted to $\delta^{18}\text{O}_{\text{VPDB}}$ using the equation from Coplen et al. (1983). At the beginning of the analysis session, a comparison of UWC-3 and the aragonite standard UWArg-7 ($\delta^{18}\text{O} = 19.73\text{‰}$ VSMOW; Linzmeier et al., 2016) identified the session-specific instrumental bias between aragonite and calcite to be 1.0‰.

Following the SIMS session, analytical metrics from each $\delta^{18}\text{O}$ analysis were evaluated for quality control, including relative yield, OH/O, and internal precision (Wycech et al., 2018). As in prior studies, outliers were identified by the Tukey outlier formula (Tukey, 1977) and, in total, 15 analyses were eliminated from the plots and discussion that follows. Detailed reporting of all raw SIMS results, including quality control metrics, are available in Table S1 of Supporting Information S1.

In addition to oxygen isotope measurements, we also collected OH/O ratios, which we assume represent relative H content (water and organic matter) trapped in the mollusk nacre across the pearl transects (Linzmeier et al., 2016; Orland et al., 2015; Wycech et al., 2018).

2.3. Scanning Electron Microscopy (SEM) and Nacre Thickness

The sampling pits of transects measured by SIMS were imaged using back-scattered electron imaging (BSE) with a FEI NOVA NanoSEM 600 scanning electron microscope. Individual pits were imaged at approximately 10,000 \times magnification using ultra high-resolution (UHR) mode with a through-the-lens detector at a working distance of 3 mm. The average thickness of nacre tablets at each SIMS pit was calculated by counting the number of tablet layers extending in a ~ 10 μm interval (approximately the diameter of a SIMS pit) measured precisely by SEM.

2.4. Confocal Raman Spectroscopy

Confocal Raman spectroscopy allowed us to map relative changes in the vibrational modes of the carbonate groups in our nacre samples on a sub-millimeter scale. Maps of confocal Raman spectra were created at Smithsonian National Museum of Natural History in the Department of Mineral Sciences using a Horiba LabRAM Evolution Raman system and CCD detector with an unpolarized 785 nm red laser coupled with a 600 groove (500 nm) grating. Spectra were collected across 50–2,000 cm^{-1} Raman shift in order to capture low-wavenumber, ν_4 , and ν_1 carbonate vibrational modes. Each $\sim 0.5 \times 3$ mm map took approximately 10 hr to collect with map grids created at 30×30 μm resolution using a $5\times$ objective lens along regions parallel and directly adjacent to the SIMS transects. Each point on the map was collected in duplicate for 2 s at a full laser power (no neutral density filters) of approximately 21 mW. The spot size of the laser using the $5\times$ objective was less than 50 μm in diameter. The laser was calibrated using a Si wafer before each map was collected and power measurements were collected before and after each map run to assure that power levels did not drift substantially during the map collection period. Laser power measurements were collected using a ThorLabs S170C Microscope Slide Power Sensor system on a silicon wafer.

All spectra were processed using LabSpec6 software and were smoothed by one point and background-subtracted using a 66-degree polynomial and 256 points. Maps of the processed spectra were created based on peak heights, full-width at half-maxima (FWHM), and peak positions of vibrational modes for aragonite at 143 cm^{-1} (defined between 139 and 144 cm^{-1}), 153 cm^{-1} (145–165 cm^{-1}), 180 cm^{-1} (170–190 cm^{-1}), the ν_4 modes at 701 and 705 cm^{-1} (698–704 cm^{-1} and 703–710 cm^{-1} , respectively), the ν_2 mode at 852 cm^{-1} (850–855 cm^{-1}), and the ν_1 mode at 1,085 cm^{-1} (1,080–1,090 cm^{-1}). Data from the Raman maps were then integrated by row and presented as transects in pearl nacre space, mirroring the SIMS transects.

To demonstrate the reproducibility of these maps and to confirm that the patterns are due to the sample and not due to fluctuations in laser power or other instrument variables, we mapped Sample 2 again on a different day with slightly different parameters (Figure S1 in Supporting Information S1) and at a horizontal orientation (Figure S2 in Supporting Information S1).

2.5. Environmental Data

All environmental data were provided by the Kentucky Lake Long-Term Monitoring Program Database run by the Hancock Biological Station, Murray State University, Murray, Kentucky, 42071. Measurements were collected in biweekly intervals from Station WP-Prairie Creek at Kentucky Lake (~ 80 km upstream from the pearl farm). For each time point, values are averaged from measurements collected at the lake surface, ~ 1 , ~ 2 , and ~ 3 m depths with errors representing the standard deviation in these depth measurements. In addition to lake water temperature ($^{\circ}\text{C}$) measurements, we explore the following environmental parameters: dissolved oxygen, total alkalinity, reduction potential, conductivity, light at 1 m, depth for 1% light, dissolved organic nitrogen, ammonia, nitrate and nitrite, silica, chlorine, sulfate, total phosphorous, and dissolved total phosphorous (see Table S2 in Supporting Information S1 for all environmental data presented in transect-space).

Environmental data were aligned to SIMS spots based on the strong relationship between $\delta^{18}\text{O}_{\text{Arg}}$ and temperature. We made the following assumptions in our data alignment: (a) small offsets of 4–20 days that are sometimes observed in other studies between temperature signals and the time that isotopic signals appear in mollusk aragonite (Vihtakari et al., 2016) are negligible in the scale of our analyses. (b) Based on previous polyphyletic observations by Dettman et al. (1999), Yoshimura et al. (2010), and Goodwin et al. (2019) that freshwater bivalve shell growth effectively pauses when water temperatures drop below approximately 10°C , we similarly removed

timeframes in the environmental data during each year between late fall when temperatures first dropped below 10°C, until spring when temperatures rose back to above 10°C. Clipped temperature data and corresponding environmental data were then linearly interpolated across nacre space such that temperature minima corresponded to $\delta^{18}\text{O}_{\text{Arg}}$ maxima (Figure S3 in Supporting Information S1). (c) While it is understood that growth rates may vary across time (e.g., Vihtakari et al., 2016), for the sake of simplicity we assume that nacre growth rate was constant between each $\delta^{18}\text{O}_{\text{Arg}}$ maxima. Since the goal of this study is to observe robust environmental signals in the nacre, we expect that any such signals should be sufficiently captured using these assumptions.

Kentucky Lake water $\delta^{18}\text{O}$ values ($\delta^{18}\text{O}_{\text{water}}$) are extrapolated from representative $\delta^{18}\text{O}_{\text{water}}$ values averaged from Ledbetter Creek (10-L) and Ledbetter Embayment (4-L) presented for several different months by Aseltyne et al. (2006) to match our approximate dates represented in the pearl transects (Table S2 in Supporting Information S1). Since we have removed dates where temperatures drop below 10°C, the range in lake $\delta^{18}\text{O}_{\text{water}}$ is less than 1‰. Still, uncertainties in how well these Aseltyne et al. (2006) water data match to values where the pearls actually grew may be higher; we assume a 2‰ uncertainty to account for potential hydrologic differences between these sites that are ~80 km apart.

2.6. Statistics

Pearson correlation matrices expressed as coefficients of determination (R^2), correlation coefficients (R), and statistical significance (p) were created to determine how all variables relate to one another for all “A” transects and for Sample 2 (Table S3 in Supporting Information S1). All Pearson correlations were run using XLSTAT software. We assume that p values below 0.05 indicate that a relationship is statistically significant. Due to the environmental nature of these samples and variables, we consider Pearson correlation coefficients (R -values) of over 0.3 represent “moderate” correlations, while values above 0.7 represent strong correlations. In addition to A-transects and Sample 2, correlations between all samples and all transects (including debris-interrupted B-transects), and for Samples 1 and 3 can also be found in Table S3 of Supporting Information S1.

3. Results and Discussion

3.1. $\delta^{18}\text{O}$ Isotope Signals Across Pearl Nacre Transects

It has been well-established that $\delta^{18}\text{O}_{\text{Arg}}$ measurements in natural biocarbonates primarily reflect environmental temperature conditions and the $\delta^{18}\text{O}_{\text{water}}$ of ambient water (e.g., Dettman et al., 1999; Yoshimura et al., 2010). We likewise demonstrate that peaks of higher $\delta^{18}\text{O}_{\text{Arg}}$ values can be matched with lake temperature lows (Figure 3, gray bars) across four growth seasons in Sample 2 (Figure S4 in Supporting Information S1), as well as for two growth seasons for Samples 1 and 3 (Figures S5–S7 in Supporting Information S1).

As expected from our data alignment based on $\delta^{18}\text{O}_{\text{Arg}}$ -temperature relationships, we observe strong negative relationships between Kentucky Lake temperature and observed $\delta^{18}\text{O}_{\text{Arg}}$ values across all “A” transects ($R^2 = 0.514$), Sample 2 ($R^2 = 0.414$), and the other samples (Figure 4a; Figure S8 and Table S3 in Supporting Information S1 for Pearson correlations). Comparing this relationship with that of predicted $\delta^{18}\text{O}_{\text{Arg}}$ values calculated from the measured lake temperatures and $\delta^{18}\text{O}_{\text{water}} = -5.58$ ‰ (Aseltyne et al., 2006), we observe that predicted $\delta^{18}\text{O}_{\text{Arg}}$ values are consistently higher than our measured values for all samples by $\sim 1.8 \pm 1$ ‰ based on Kim et al. (2007), and $\sim 2.4 \pm 1$ ‰ based on Grossman and Ku (1986). This offset relationship is illustrated as $1000\ln\alpha_{\text{Arg-water}}$ versus formation temperature in Figure 4b and matches a well-documented ~ 2 ‰ offset between SIMS-based and acid digestion-based measurements of modern bio-aragonite due in part to a lack of matrix-matched standards (amount of water and organic matter). Given this systematic uncertainty, we assume that vital effects are negligible in these samples (Orland et al., 2015), but any vital effect would contribute to these differences. The offset shown in Figure 4b may also be partially driven by an imprecision in matching temporal environmental data to precise nacre layers. Considering how well the patterns of observed and temperature-predicted $\delta^{18}\text{O}$ measurements align, especially compared to other environmental studies, we assume that they are sufficiently aligned to proceed with further environmental and mineralogical comparisons.

By building on the $\delta^{18}\text{O}_{\text{Arg}}$ -temperature relationship, we were able to compare $\delta^{18}\text{O}_{\text{Arg}}$ and other shell variables to the Kentucky Lake environmental data set. Increasing $\delta^{18}\text{O}_{\text{Arg}}$ values are correlated with lower OH/O ratios in nacre aragonite, as well as with lower light levels measured at 1 m depth and higher dissolved oxygen levels in

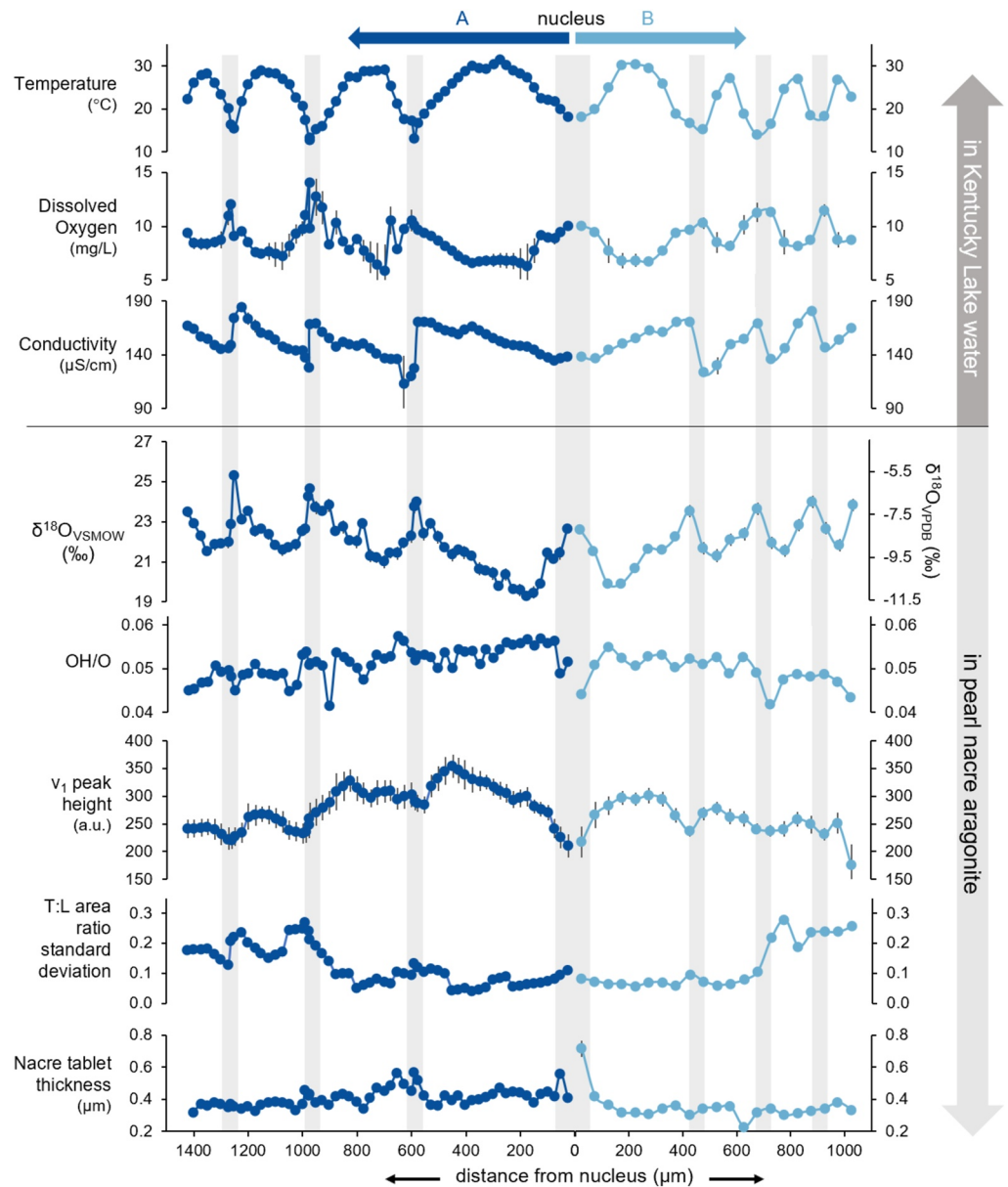


Figure 3. A selection of environmental variables at Kentucky Lake compared to measurements of SIMS-based oxygen isotope ratios and OH/O, Raman spectroscopy-based carbonate bonding environments, and nacre tablet thickness expressed as relative values along mirroring A and B transects across Sample 2. Seasonal cycles over four years of growth defined by lake temperature lows and $\delta^{18}\text{O}_{\text{Arg}}$ maxima are highlighted in gray bars across all variables. Error bars represent measurement precision for SIMS data and nacre tablet thickness, and estimated standard deviations for environmental data and Raman-based data. For the complete data set for all samples and variables, see Table S2, as well as Figure S4 in Supporting Information S1 for a more detailed version of this figures and Figures S5 and S6 in Supporting Information S1 for similar figures for Samples 1 and 3.

Kentucky Lake (Figures 4c–4e). These statistically significant relationships ($p < 0.0001$; Pearson correlations in Table S3 of Supporting Information S1) were observed across the more pristine (inclusion-free) “A” transects of all three pearl samples (black open circles), as well as across both pristine transects in Sample 2 (blue circles). R^2 values for these relationships appear to be higher in Sample 2 compared to the other samples. These environmental trends make sense in a seasonal context where colder waters hold higher concentrations of dissolved oxygen and experience lower light levels in winter. It also implies that the mechanisms that create the OH/O signals in nacre (i.e., water and/or organic compounds) are similarly seasonally impacted.

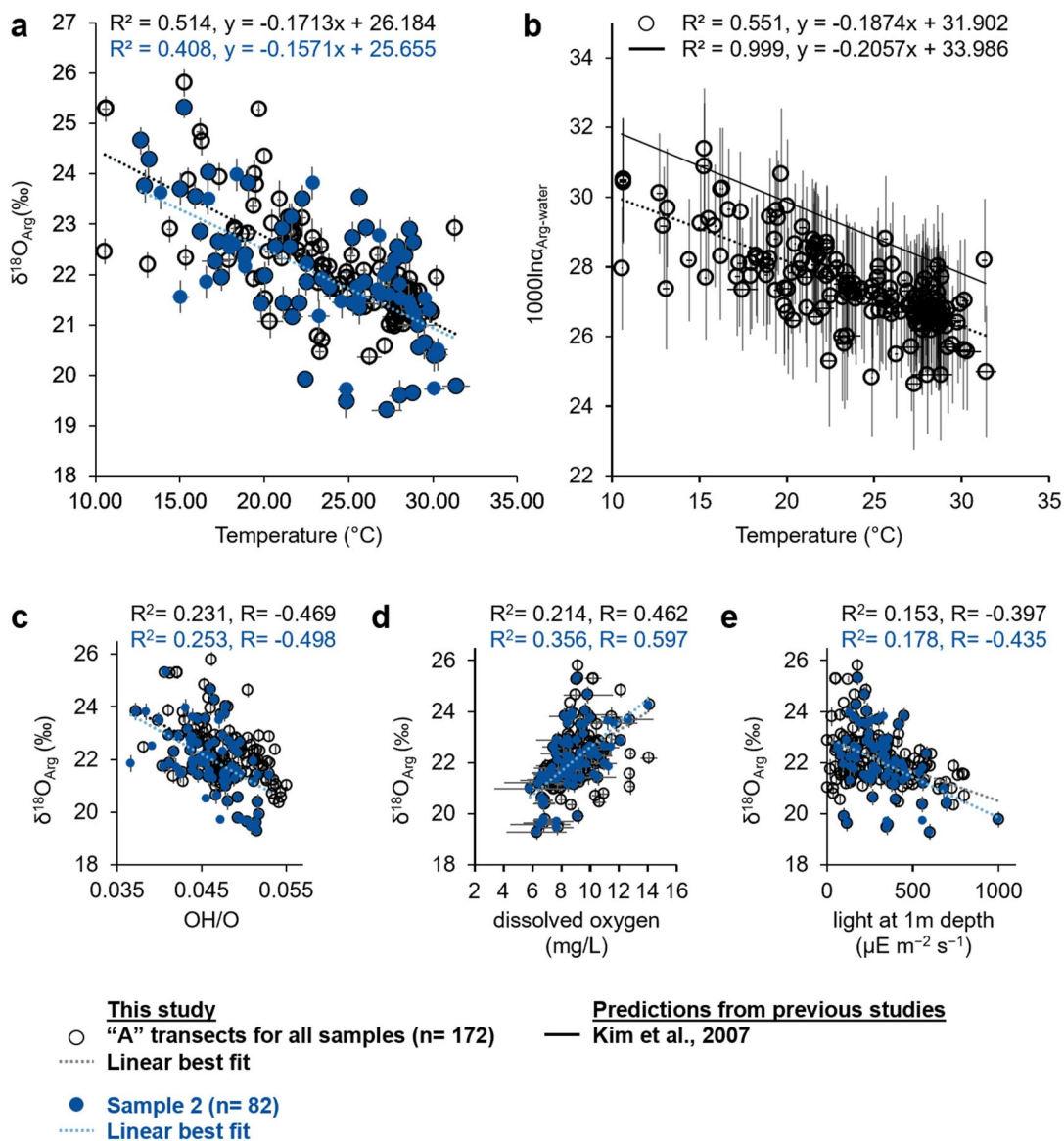


Figure 4. (a) Measurements of $\delta^{18}\text{O}_{\text{Arg}}$ (VSMOW) for “A” transects and for Sample 2 (Figure 2) as a function of temperature. (b) $1000\ln\alpha_{\text{Arg-water}}$ predicted for the “A” transects in this study, as well as values based on fractionation factors of Kim et al. (2007) as a function of Kentucky Lake temperature. We assume $1000\ln\alpha_{\text{Arg-water}}$ with water values extrapolated from Aseltyn et al. (2006) (Table S2 in Supporting Information S1). Measurements of $\delta^{18}\text{O}_{\text{Arg}}$ (VSMOW) as a function of (c) SIMS-based OH/O ratios, (d) dissolved oxygen in Kentucky Lake, and (e) light levels at 1 m depth in Kentucky Lake. Error bars represent precision in the isotopic and environmental measurements. All relationships represented are statistically significant with p -values of <0.0001 .

3.2. Nacre Tablet Thickness

Nacre is a biomineral composite material of aragonite, chitin, and other biomolecules formed in layers where each aragonite tablet crystal is oriented with the c -axis parallel to the direction of pearl growth (e.g., Marin et al., 2012). Unlike coral aragonite needles, nacre tablets are suppressed from growing along the c -axis and preferentially extend along the a - and b -axes to create a flat, tablet shape (Checa et al., 2013; Saruwatari et al., 2009). Observations of mollusks across geologic time have reported that average nacre tablet thickness is positively correlated with increasing nacre formation temperatures (Gilbert et al., 2017) and negatively correlated with increasing hydrostatic pressure; however, this mineralogical proxy has not yet been extensively applied to shifts in nacre tablet thickness measurements in natural samples over modern seasonal timescales (Olson et al., 2012).

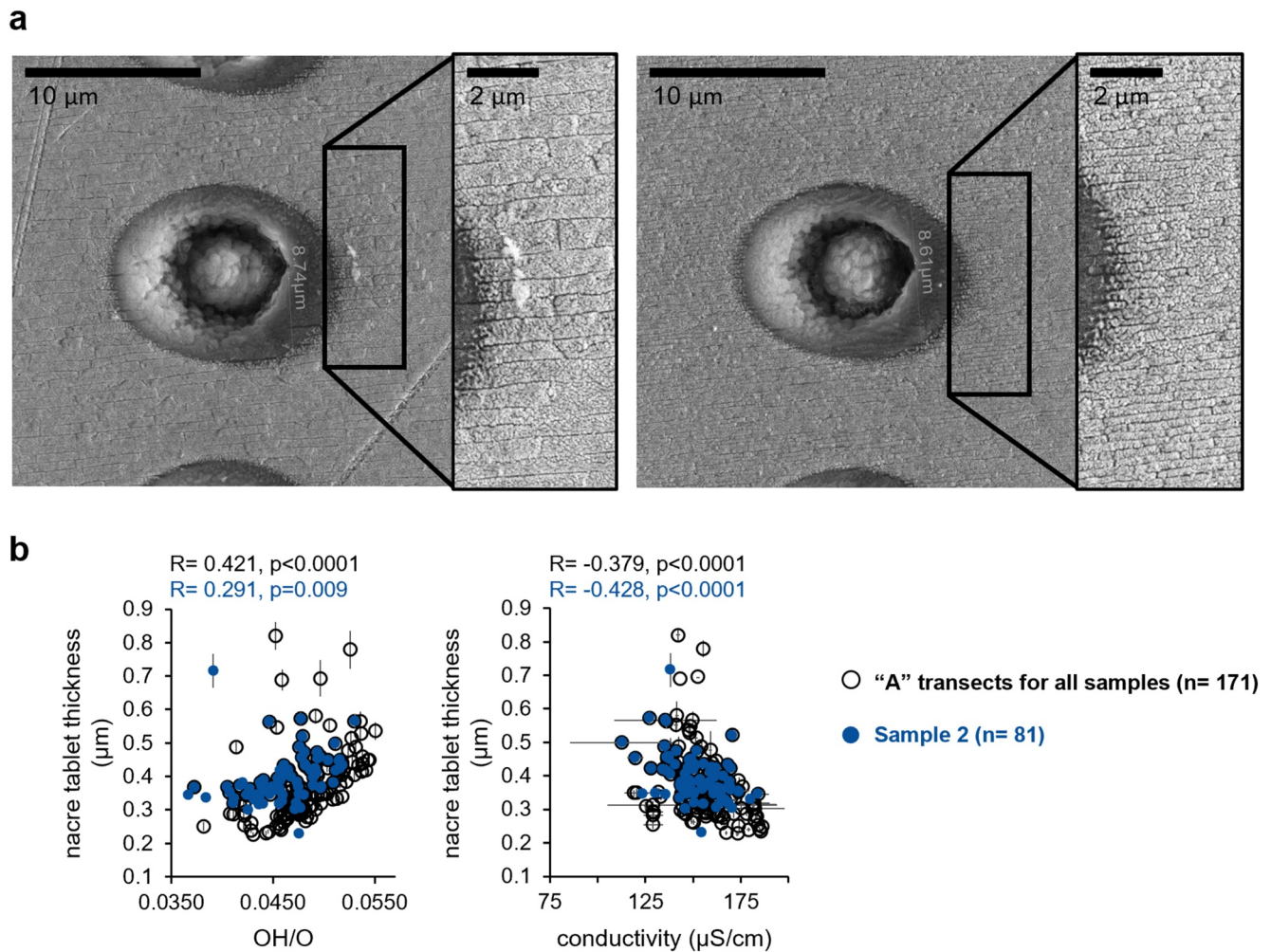


Figure 5. (a) Back-scattered electron (BSE) images of SIMS pits collected across freshwater cultured pearl nacre from near Kentucky Lake. Zoomed-in views of the nacre tablets adjacent to the SIMS pits highlight the difference in nacre tablet thickness across different regions of the pearl. (b) Correlations between nacre tablet thickness and OH/O ratios taken via SIMS and for electrical conductivity measurements of Kentucky Lake for all “A” transects and for Sample 2. Error bars represent precision of measurements.

In this study, we observe that nacre thickness (illustrated in Figure 5a) may vary by a factor of up to approximately 6X across a single pearl transect (Figure S9 in Supporting Information S1). In Sample 2, tablet thickness varied by ~3X, ranging from 0.23–0.72 μm. These shifts in nacre thickness do not appear to reflect the same seasonal patterns as temperature and $\delta^{18}\text{O}_{\text{VSMOW}}$ measurements in Sample 2 (Figure 3) or in the other samples (Figures S4, S5, and S8 in Supporting Information S1). In fact, thicker nacre tablets are found in some growth zones from the coldest months (Figure 3)

Instead of following seasonal temperature patterns, we observe that the nacre tablet thickness measurements in this study (for all “A” transects and for Sample 2) best correlate to increasing OH/O ratios collected with SIMS, and decreasing Kentucky Lake electrical conductivity measurements (Figure 5b). Previous studies have not measured the correlation of water conductivity (which we assume is related to salinity or ion content) to nacre thickness, however they have discovered that other variables such as chlorophyll (a measure for food abundance) may be positively correlated to faster growth rates and thicker nacre tablets (Tomaru et al., 2002).

Another notable observation on nacre thickness is that in the areas closest to the nucleation site, the nacre is not organized as clear tablets, but rather as asymmetrical polygon patterns that are much wider than even the widest nacre tablets (Figure S10 in Supporting Information S1). We also find that the tablets that develop closer to the nucleus tend to be thicker, regardless of formation temperature (Figure 3; Figure S9 in Supporting Information S1).

Table 1
Mean Values (\pm e.s.d.) of Raman Peak Positions for “A” Transects and Sample 2, as Well as for all Samples and Samples 1 and 3

This study	<i>n</i>	143 cm ⁻¹ peak	153 cm ⁻¹ peak	180 cm ⁻¹ peak	206 cm ⁻¹ peak	701 cm ⁻¹ ν_4 peak	705 cm ⁻¹ ν_4 peak	852 cm ⁻¹ ν_2 peak	1,085 cm ⁻¹ ν_1 peak
A transects	172	142.93 \pm 0.23	152.3 \pm 0.27	179.54 \pm 0.29	205.57 \pm 0.24	701.8 \pm 0.8	704.99 \pm 0.17	852 \pm 9	1,085.04 \pm 0.07
Sample 2	82	142.93 \pm 0.22	152.61 \pm 0.14	179.78 \pm 0.18	205.87 \pm 0.13	701.3 \pm 0.4	705.19 \pm 0.12	853.1 \pm 0.3	1,085 \pm 0.01
All samples	308	142.6 \pm 0.6	152.23 \pm 0.3	181 \pm 2.7	205.8 \pm 1	701.8 \pm 0.6	704.88 \pm 0.27	852.3 \pm 5.8	1,085.02 \pm 0.07
Sample 1	162	142.4 \pm 0.6	152.03 \pm 0.18	182.2 \pm 3.3	205.9 \pm 1.3	702.01 \pm 0.5	704.68 \pm 0.17	852 \pm 8	1,085 \pm 0.01
Sample 3	64	142.94 \pm 0.33	152.27 \pm 0.18	179.55 \pm 0.51	205.51 \pm 0.12	702.1 \pm 0.8	704.98 \pm 0.13	852.93 \pm 0.28	1,085.11 \pm 0.12

Previous studies	Sample	143 cm ⁻¹ peak	153 cm ⁻¹ peak	180 cm ⁻¹ peak	206 cm ⁻¹ peak	701 cm ⁻¹ ν_4 peak	705 cm ⁻¹ ν_4 peak	852 cm ⁻¹ ν_2 peak	1,085 cm ⁻¹ ν_1 peak
Urmos et al. (1991)	Natural pearl	143	153 (7.4)	180 (5.6)	206 (6.8)	701	705	852	1,085 (2.1)
	Cultured pearl	144	153 (8.7)	180 (6.0)	206 (7.4)	701	705		1,085 (2.2)
Nehrke and Nouet (2011)	<i>Nerita undata</i>		152		206		705		1,085
Beierlein et al. (2015)	<i>Arctica islandica</i>		152		206		705		1,085

Note. These values are compared to peak position values from previous studies on freshwater mollusks (Beierlein et al., 2015; Nehrke & Nouet, 2011; Urmos et al., 1991).

To compare to previous studies which used average nacre thicknesses to predict water temperatures during nacre formation, we observe that the average nacre thickness measurements (\pm S.D.) across all three samples ($0.56 \pm 0.07 \mu\text{m}$, Figure 5a) predicts an average lake formation temperature of $19.5 \pm 5.8^\circ\text{C}$ using the proxy equation for marine nacre tablet thickness (μm) = $0.2830 + 0.0144 \times T$ ($^\circ\text{C}$) from Gilbert et al. (2017) which works for nacre thicknesses ranging from approximately 0.43–0.71 μm . This prediction falls close to, but slightly below, average lake temperatures actually recorded in Kentucky Lake while the nacre was being formed ($23.5 \pm 4.9^\circ\text{C}$). If we average the lake temperature across the full timeframe ($20 \pm 7^\circ\text{C}$), including when temperatures fall below 10°C , the prediction is even closer. Still, we estimate that growth pauses around 10°C since this is observed in other freshwater mussels (Dettman et al., 1999; Goodwin et al., 2019; Yoshimura et al., 2010) and it is also well-known that cultured pearl harvesting is conducted during the onset of these colder seasons, precisely due to the slower nacre growth rates and thinner nacre layers leading to higher quality luster and fewer defects in the final surface layers of the pearls (e.g., Latchere et al., 2018). Although the Gilbert et al. (2017) equation accurately predicts annual average water temperature at Kentucky Lake using the average thickness of nacre tablets in our samples, it does not accurately reconstruct seasonal temperature variability from the high-resolution spatial and temporal observations of tablet thickness in this study.

3.3. Raman Spectroscopy and Mineral Identification

Raman spectra of the pearls in this study confirm that they are composed of aragonite, with specific peaks matching observations of common carbonate group vibrational modes presented by Urmos et al. (1991) and Bischoff et al. (1985; Figure 1). Average Raman shift positions in wavenumber (cm^{-1}) for each peak are presented in Table 1 and indicate that they are comparable to results from previous mollusk Raman studies (Beierlein et al., 2015; Nehrke & Nouet, 2011; Urmos et al., 1991). In this study, we see no evidence of other carbonate phases, such as calcite or vaterite which have been observed and mapped by Raman spectroscopy in an Antarctic mollusk study (Nehrke et al., 2012), or amorphous calcium carbonate (ACC) observed via Raman spectroscopy in larval bivalves (Ramesh et al., 2018) or via coupled photoemission electron spectromicroscopy (PEEM) and X-ray absorption near-edge structure (XANES) in fresh red abalone (DeVol et al., 2015). Since we used a red 785 nm laser for our measurements, and the pearls in our study are white and unpigmented, we did not observe clear Raman signatures for pigments (or vaterite associated with some of these pigments) described in previous studies on pigmented saltwater and freshwater pearls (Karampelas et al., 2019; Soldati et al., 2008).

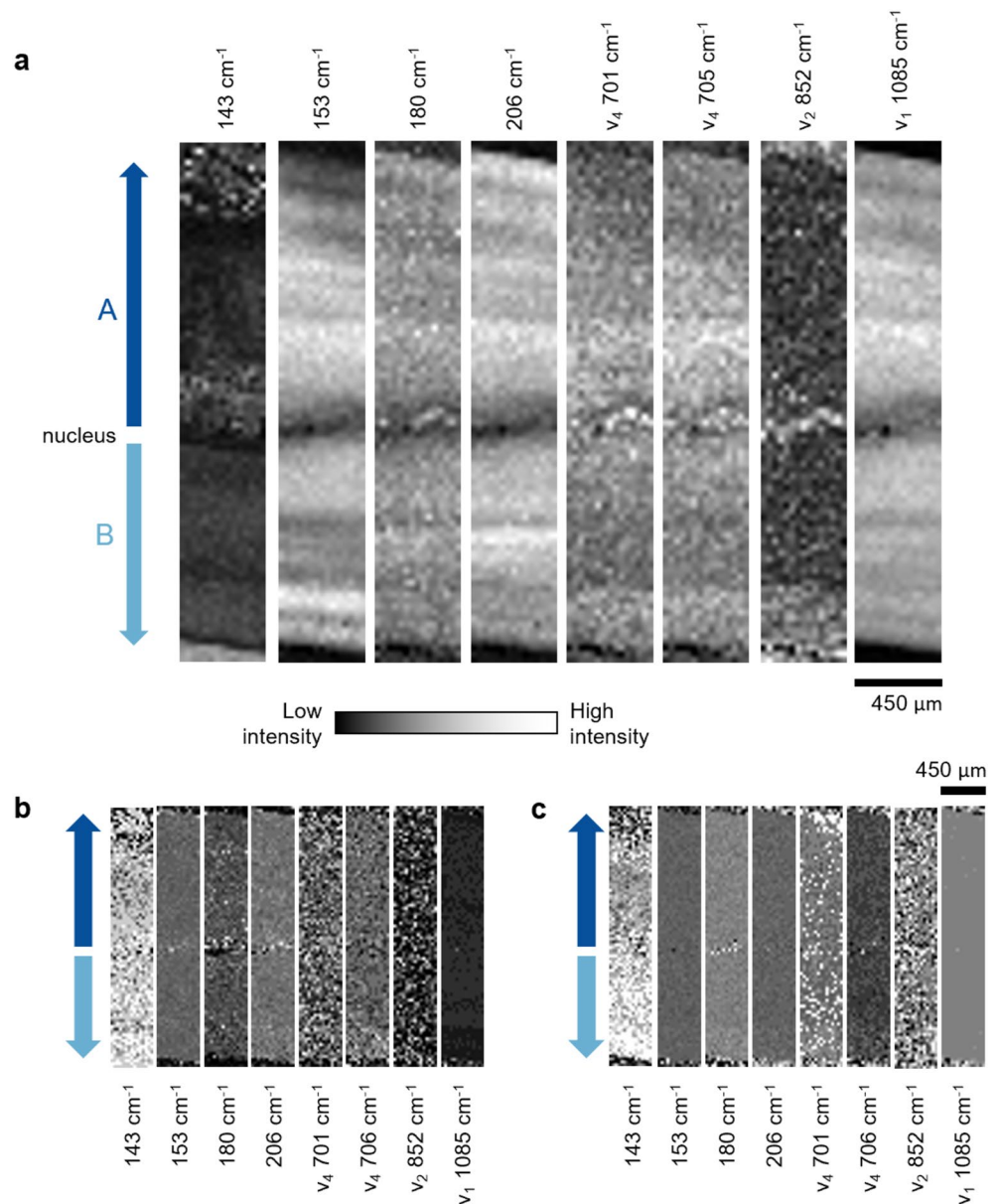


Figure 6. Maps of features in background-subtracted Raman spectra collected of the region alongside the SIMS A and B transects across Sample 2 (see Figure 2). Each map is for an individual peak representing the vibrational modes depicted in Figure 1. Each pixel represents a $30 \times 30 \mu\text{m}$ box. (a) Maps of Raman peak height intensities (arbitrary units). Light-colored high intensities represent relatively taller peaks. (b) Maps of Raman peak FWHMs (cm^{-1}) with light-colored high intensities representing wider peaks. (c) Maps of Raman peak positions (cm^{-1}) with light-colored high intensities representing higher wavenumber Raman shifts.

3.4. Raman Peak Height Intensity Maps and Seasonal Environmental Variables

Our two-dimensional maps of Raman peak height intensities visually indicate that peak heights follow heterogeneous patterns that mirror each other across the A and B pearl growth transects (Figure 6a; Figures S11a and S12a in Supporting Information S1). This is particularly clear for the dominant ν_1 mode, the 153 cm^{-1} translational mode, and the ν_4 mode peak heights (Figure 3, Figure S13 in Supporting Information S1). We observe a moderate positive correlation between increasing ν_1 peak intensities with increasing Kentucky lake temperature for A-transects, and a consistent (but weaker) correlation within Sample 2 (Figure 7a).

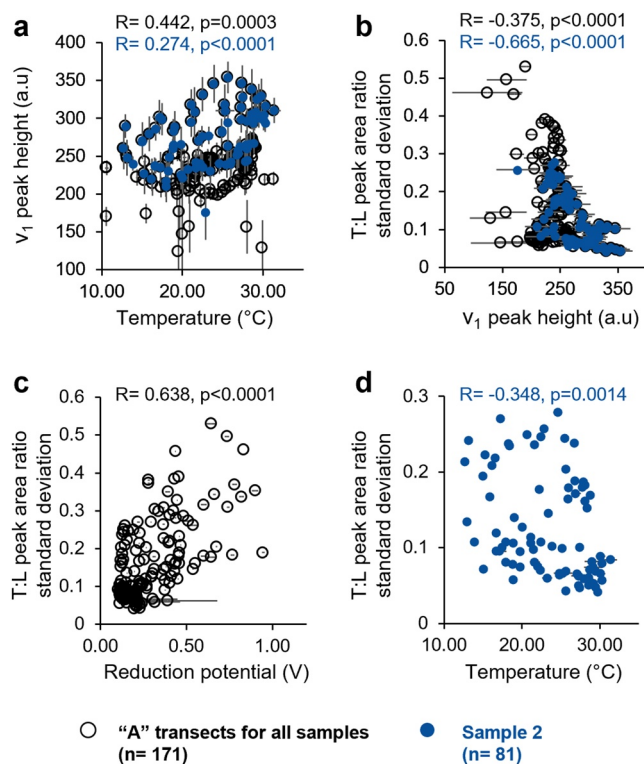


Figure 7. Raman spectroscopy results of A-Transects of all three pearl samples (black open-circles, $n = 172$) as well as of Sample 2 (transects A and B, blue circles, $n = 82$) for (a) ν_1 Raman mode peak heights correlated to Kentucky Lake temperature and for (b) carbonate translational mode:librational mode (T:L) peak area ratio standard deviations (representing nacre tablet crystalline disorientation) correlated to ν_1 Raman mode peak heights. T:L peak area standard deviations are also correlated to (c) Kentucky Lake reduction potential for A-transects and (d) Kentucky lake temperature for Sample 2. Error bars represent precision of measurements for environmental data and estimated standard deviations for Raman data.

Unlike the clear patterns in our maps of Raman peak heights, we do not see clear oscillations in T:L ratios across pearl transects resembling the seasonal cycles we are looking for (Figure S14 in Supporting Information S1). Although we do not have access to PIC mapping in this study, here we take a novel Raman-based approach to uncover similar information on relative crystallographic orientation. Assuming that T:L ratios are indicative of crystallographic orientation, we further assume that the standard deviation in Raman T:L ratios across our 2D map integrations can approximate relative disorientation in nacre tablet alignment across our maps. This calculation does yield seasonal-scale changes across the pearl nacre with local minima which approximately align with the local maxima of direct peak height measurements (Figure 3; Figures S4 and S13 in Supporting Information S1). Correlating this crystalline disorientation measurement with other variables reveals that T:L peak area ratio standard deviations negatively correlate with higher ν_1 mode peak intensities in both A-transects and in Sample 2 (Figure 7b) and positively correlate to increasing reduction-oxidation potential at Kentucky Lake for pearl A-transects (Figure 7c; Table S2 in Supporting Information S1). Within Sample 2, Raman-based T:L standard deviations correlate with Kentucky Lake water temperature; however, unlike crystal angle spread observations in Olson and Gilbert (2012) and previous studies relating nacre microstructure to temperature (Gilbert et al., 2017), these relationships do not extend to the “A” transects in the other samples (Figure 7d). This may be due to freshwater nacre aragonite mineralogy not being as strongly impacted by temperature shifts, or, since the pearls in this study were not grown in the precise location and timeframes as the lake environmental data, they may not reflect the same temperature fidelity as incubation experiments or broader averages.

Aligning our Raman height measurements with our other mineralogical and chemical proxies and environmental data, we visually observe that peak height patterns mimic seasonal cycles, yet they may not always be directly correlated (Figure 3; Figures S4–S6 in Supporting Information S1). Beyond relationships with temperature, our multivariable approach enables us to observe several other relationships with nacre mineralogy which appear to be more robust (i.e., dissolved oxygen, electrical conductivity, reduction potential; Table S1 in Supporting Information S1). Figures 8a–8c highlight how ν_4 and ν_1 peak heights may be reasonably correlated to the $\delta^{18}\text{O}$ proxy, which is a known robust temperature proxy given that the $\delta^{18}\text{O}$ of lake water is nearly constant. These same peak heights are also correlated to dissolved oxygen levels in Kentucky Lake (Figures 8d–8f). All other potential correlations between Raman signals and environmental data and proxies can be seen in the Pearson correlation matrices (Table S3 in Supporting Information S1).

Considering that Raman ν_1 mode peak heights are correlated to both nacre $\delta^{18}\text{O}$ and dissolved oxygen in Kentucky Lake (Figures 3 and 8), the effect of dissolved oxygen on $\delta^{18}\text{O}$ in biocarbonates should be further explored. We observe that colder waters with high concentrations of dissolved oxygen correlating with higher $\delta^{18}\text{O}_{\text{Arg}}$ ratios (Figure 4d) align with regions of nacre with shorter Raman mode peak heights (Figures 3 and 8). This lower-intensity Raman signal indicates less-concentrated aragonite, likely due to higher organics:aragonite ratios. This may indicate periods of slow-growth or paused nacre growth with more layers and presumably more inter-layer organics during these colder seasons. Future studies should directly investigate the incorporation of organics in this mineralogical and isotopic context. This relationship with dissolved oxygen is also particularly striking since it is well known that mollusk health is related to dissolved oxygen levels, and that sensitive mollusk species can only thrive in waters with higher levels of dissolved oxygen (Kuk-Dzul & Díaz-Castañeda, 2016).

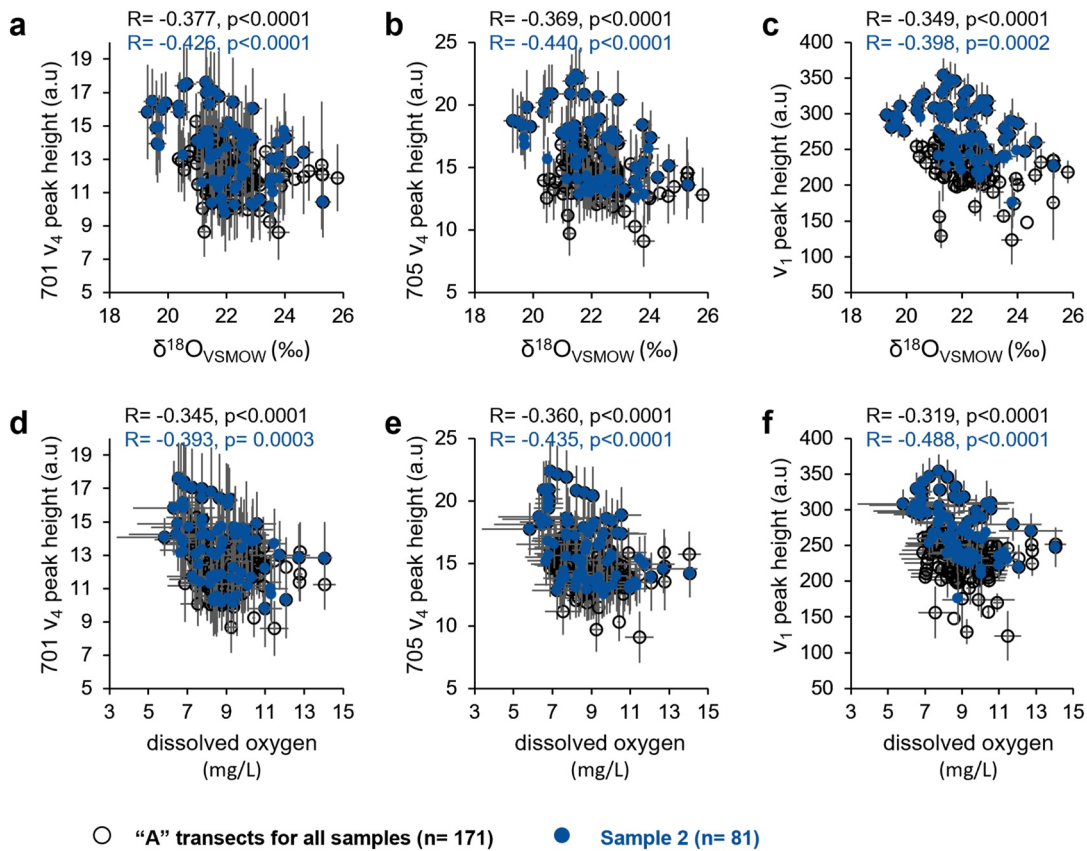


Figure 8. Correlations between Raman peak height intensities for ν_4 mode peaks at 701 cm^{-1} and at 705 cm^{-1} and the ν_1 mode at $1,085\text{ cm}^{-1}$, respectively, and (a–c) $\delta^{18}\text{O}_{\text{VSMOW}}$ nacre measurements and (d–f) dissolved oxygen in Kentucky Lake for A-Transects (black, $n = 172$) and Sample 2 (blue, $n = 82$). Error bars represent measurement errors for SIMS and environmental data and estimated standard deviations for Raman data.

3.5. Raman Peak FWHM and Aragonite Saturation State

In contrast to the clearly heterogeneous signals in Raman peak heights, heterogeneity is not seen for peak FWHMs or peak positions, which remain relatively homogenous across the growth history of the pearl (Figures 6b and 6c; Figures S11b, S11c, S12b, and S12c in Supporting Information S1). The exception is when a transect is interrupted by large organic material inclusions (highlighted dashed arrows in Figure 2) which may express varying peak FWHMs and peak positions around the inclusion (Figures S11b, S11c, S12b, and S12c in Supporting Information S1). Previous Raman studies on coral aragonite have used the FWHM of the ν_1 mode as a measure of aragonite saturation state (Ω_{Arg}) in the coral calcifying fluid (DeCarlo et al., 2017; Farfan et al., 2018). Assuming that the same relationship holds true for freshwater mollusks, the homogenous nature of ν_1 FWHMs across these pearls suggests that mollusk calcifying Ω_{Arg} remains constant across seasonal changes in the environment. This aligns with previous studies that have proposed that mollusk nacre aragonite forms by amorphous calcium carbonate (ACC) precursor phases (Addadi et al., 2006; Checa et al., 2013; Dauphin, 2001; DeVol et al., 2015). Furthermore, only a weak-to-moderate correlation between alkalinity (our closest parameter to environmental Kentucky Lake Ω_{Arg}) and ν_1 FWHM exists for A-transects with a correlation coefficient R value of 0.318 (Table S3 in Supporting Information S1). Assuming that this relationship applies to mollusks and is irrespective of biomineralization mechanism, the ν_1 FWHM averaged across all samples in this study is approximately 2.6 cm^{-1} , which would calculate an Ω_{Arg} of formation of 2.45 for this pearl nacre. This is far below the range of values $\Omega_{\text{Arg}} > 10$ measured by DeCarlo et al. (2017) to relate to coral calcifying fluid Ω_{Arg} .

4. Conclusions

1. Our high-spatial resolution Raman maps coupled with nacre tablet thickness, nacre oxygen isotope ($\delta^{18}\text{O}$) measurements by SIMS, and environmental data from Kentucky Lake demonstrate that micro-scale mineralogical features in pearls show promise as proxies for seasonal resolution paleoenvironmental conditions.
2. Raman spectroscopy maps of ν_1 and ν_4 carbonate vibrational modes show seasonal variations in peak heights that correlate with the $\delta^{18}\text{O}_{\text{Arg}}$ proxy for temperature, as well as with direct measurements for dissolved oxygen in Kentucky Lake. Thus, Raman maps may be used to help non-destructively track yearly growth bands in pearls and to make inferences about the local environment.
3. We present novel Raman-based translational:librational (T:L) mode peak area ratio standard deviations as an approximation for relative nacre tablet crystallographic disorientation.
4. Relationships between nacre mineralogy and temperature in these freshwater pearls are not as straightforward as proposed in previous studies of marine mollusk nacre tablet thicknesses and orientations as a function of temperature. Instead, nacre tablet thickness correlates with lake conductivity and relative nacre OH/O ratios measured by SIMS.
5. Beyond temperature, higher $\delta^{18}\text{O}_{\text{Arg}}$ values correlate with decreasing relative nacre OH/O ratios, increasing dissolved oxygen levels in Kentucky lake, and decreasing light levels at 1 m depth in Kentucky Lake, which are all likely linked to seasonal changes in the lake.
6. To quantify Raman signals as an independent mineralogical proxy, we suggest that future incubation experiments precisely correlate temperature and other environmental parameters to Raman spectroscopy peak height and peak ratio signals in freshwater mollusk systems and beyond.

Conflict of Interest

The authors declare no conflicts of interest relevant to this study.

Data Availability Statement

All data for this study is available in Tables S1–S3 of Supporting Information S1 and through Pangea (<https://doi.pangaea.de/10.1594/PANGAEA.938370>).

Acknowledgments

The authors would like to thank Gina Latendresse and the Latendresse family of the American Pearl Company, Inc. for the pearl samples and for insights about pearl culturing and harvesting, Tim Gooding and Rob Wardell for helping prepare the samples, setup for SEM imaging, and with Raman spectroscopy, and Xulong Peng and Michael Flinn for granting us access to data from the The Kentucky Lake Long-Term Monitoring Program Database at Murray State University, KY, which is supported by the Hancock Biological Station (HBS) and Watershed Studies Institute (WSI). This project was funded by the Smithsonian NMNH Coralyn Wright Whitney Curator of Gems and Minerals Endowment and the Gemological Institute of America. WiseSIMS is supported by NSF (EAR-1658823, 2004618) and UW-Madison.

References

- Abell, P. I. (1985). Oxygen isotope ratios in modern African gastropod shells: A data base for paleoclimatology. *Chemical Geology: Isotope Geoscience Section*, 58(1–2), 183–193. [https://doi.org/10.1016/0168-9622\(85\)90037-5](https://doi.org/10.1016/0168-9622(85)90037-5)
- Addadi, L., Joester, D., Nudelman, F., & Weiner, S. (2006). Mollusk shell formation: A source of new concepts for understanding biomineralization processes. *Chemistry—A European Journal*, 12(4), 980–987. <https://doi.org/10.1002/chem.200500980>
- Aselyte, T. A., Rowe, H. D., & Fryar, A. E. (2006). Stable isotopic fingerprint of a hyporheic–hypolentic boundary in a reservoir. *Hydrogeology Journal*, 14(8), 1688–1695. <https://doi.org/10.1007/s10040-006-0088-2>
- Beierlein, L., Nehrke, G., & Brey, T. (2015). Confocal Raman microscopy in sclerochronology: A powerful tool to visualize environmental information in recent and fossil biogenic archives. *Geochemistry, Geophysics, Geosystems*, 16(1), 325–335. <https://doi.org/10.1002/2014GC005547>
- Biellmann, C., & Gillet, P. (1992). High-pressure and high-temperature behaviour of calcite, aragonite and dolomite: A Raman spectroscopic study. *European Journal of Mineralogy*, 4, 389–394. <https://doi.org/10.1127/ejm/4/2/0389>
- Bischoff, W. D., Sharma, S. K., & MacKenzie, F. T. (1985). Carbonate ion disorder in synthetic and biogenic magnesian calcites: A Raman spectral study. *American Mineralogist*, 70(5–6), 581–589.
- Cahn, A. R. (1949). *Pearl culture in Japan. Fishery Leaflet* (Vol. 357). US Fish and Wildlife Service.
- Checa, A. G. (2018). Physical and biological determinants of the fabrication of molluscan shell microstructures. *Frontiers in Marine Science*, 5, 353. <https://doi.org/10.3389/fmars.2018.00353>
- Checa, A. G., Mutvei, H., Osuna-Mascaró, A. J., Bonarski, J. T., Faryna, M., Berent, K., et al. (2013). Crystallographic control on the substructure of nacre tablets. *Journal of Structural Biology*, 183(3), 368–376. <https://doi.org/10.1016/j.jsb.2013.07.014>
- Coplen, T. B., Kendall, C., & Hopple, J. (1983). Comparison of stable isotope reference samples. *Nature*, 302(5905), 236–238. <https://doi.org/10.1038/302236a0>
- Dauphin, Y. (2001). Comparative studies of skeletal soluble matrices from some Scleractinian corals and Molluscs. *International Journal of Biological Macromolecules*, 28(4), 293–304. [https://doi.org/10.1016/S0141-8130\(01\)00124-6](https://doi.org/10.1016/S0141-8130(01)00124-6)
- DeCarlo, T. M., D'Olivo, J. P., Foster, T., Holcomb, M., Becker, T., & McCulloch, M. T. (2017). Coral calcifying fluid aragonite saturation states derived from Raman spectroscopy. *Biogeosciences*, 14(22), 5253–5269. <https://doi.org/10.5194/bg-14-5253-2017>
- Dettman, D. L., Reische, A. K., & Lohmann, K. C. (1999). Controls on the stable isotope composition of seasonal growth bands in aragonitic fresh-water bivalves (Unionidae). *Geochimica et Cosmochimica Acta*, 63(7–8), 1049–1057. [https://doi.org/10.1016/S0016-7037\(99\)00020-4](https://doi.org/10.1016/S0016-7037(99)00020-4)
- DeVol, R. T., Sun, C. Y., Marcus, M. A., Coppersmith, S. N., Myneni, S. C., & Gilbert, P. U. P. A. (2015). Nanoscale transforming mineral phases in fresh nacre. *Journal of the American Chemical Society*, 137(41), 13325–13333. <https://doi.org/10.1021/jacs.5b07931>

- Dickinson, G. H., Ivanina, A. V., Matoo, O. B., Pörtner, H. O., Lannig, G., Bock, C., et al. (2012). Interactive effects of salinity and elevated CO₂ levels on juvenile eastern oysters, *Crassostrea virginica*. *Journal of Experimental Biology*, 215(1), 29–43. <https://doi.org/10.1242/jeb.061481>
- Farfan, G. A., Cordes, E. E., Waller, R. G., DeCarlo, T. M., & Hansel, C. M. (2018). Mineralogy of deep-sea coral aragonites as a function of aragonite saturation state. *Frontiers in Marine Science*, 5, 473. <https://doi.org/10.3389/fmars.2018.00473>
- Freitas, P., Clarke, L. J., Kennedy, H., Richardson, C., & Abrantes, F. (2005). Mg/Ca, Sr/Ca, and stable-isotope ($\delta^{18}\text{O}$ and $\delta^{13}\text{C}$) ratio profiles from the fan mussel *Pinna nobilis*: Seasonal records and temperature relationships. *Geochemistry, Geophysics, Geosystems*, 6(4), 1–16. <https://doi.org/10.1029/2004GC000872>
- Fritz, P., & Poplawski, S. (1974). ^{18}O and ^{13}C in the shells of freshwater molluscs and their environments. *Earth and Planetary Science Letters*, 24(1), 91–98. [https://doi.org/10.1016/0012-821X\(74\)90012-0](https://doi.org/10.1016/0012-821X(74)90012-0)
- Gervis, M. H., & Sims, N. A. (1992). *The biology and culture of pearl oysters (Bivalvia pteriidae)* (Vol. 21). WorldFish.
- Gibson, R., Barnes, M., & Atkinson, R. (2001). Molluscs as archives of environmental change. *Oceanography and Marine Biology: An Annual Review*, 39, 103–164.
- Gilbert, P. U. P. A., Bergmann, K. D., Myers, C. E., Marcus, M. A., DeVol, R. T., Sun, C. Y., et al. (2017). Nacre tablet thickness records formation temperature in modern and fossil shells. *Earth and Planetary Science Letters*, 460, 281–292. <https://doi.org/10.1016/j.epsl.2016.11.012>
- Gim, J., Schnitzer, N., Otter, L. M., Cui, Y., Motreuil, S., Marin, F., et al. (2019). Nanoscale deformation mechanics reveal resilience in nacre of *Pinna nobilis* shell. *Nature Communications*, 10(1), 1–8. <https://doi.org/10.1038/s41467-019-12743-z>
- Goodwin, D. H., Gillikin, D. P., Banker, R., Watters, G. T., Dettman, D. L., & Romanek, C. S. (2019). Reconstructing intra-annual growth of freshwater mussels using oxygen isotopes. *Chemical Geology*, 526, 7–22. <https://doi.org/10.1016/j.chemgeo.2018.07.030>
- Grossman, E. L., & Ku, T. L. (1986). Oxygen and carbon isotope fractionation in biogenic aragonite: Temperature effects. *Chemical Geology: Isotope Geoscience Section*, 59, 59–74. [https://doi.org/10.1016/0168-9622\(86\)90057-6](https://doi.org/10.1016/0168-9622(86)90057-6)
- Helsler, T., Kastle, C., McKay, J., Orland, I. J., Kozdon, R., Valley, J. W. (2018). Evaluation of micromilling/conventional isotope ratio mass spectrometry and secondary ion mass spectrometry of $\delta^{18}\text{O}$ in fish otoliths for sclerochronology. *Rapid Communications in Mass Spectrometry*, 32: 1781–1790. <https://doi.org/10.1002/rcm.8231>
- Höche, N., Walliser, E. O., de Winter, N. J., Witbaard, R., & Schöne, B. R. (2021). Temperature-induced microstructural changes in shells of laboratory-grown *Arctica islandica* (Bivalvia). *PLoS One*, 16(2), e0247968. <https://doi.org/10.1371/journal.pone.0247968>
- Høie, H., Otterlei, E., & Folkvord, A. (2004). Temperature-dependent fractionation of stable oxygen isotopes in otoliths of juvenile cod (*Gadus morhua* L.). *ICES Journal of Marine Science*, 61(2), 243–251. <https://doi.org/10.1016/j.icesjms.2003.11.006>
- Kalish, J. M. (1991). Oxygen and carbon stable isotopes in the otoliths of wild and laboratory-reared Australian salmon (*Arripis trutta*). *Marine Biology*, 110(1), 37–47. <https://doi.org/10.1007/BF01313090>
- Karampelas, S., Fritsch, E., Makhloof, F., Mohamed, F., & Al-Alawi, A. (2019). Raman spectroscopy of natural and cultured pearls and pearl producing mollusc shells. *Journal of Raman Spectroscopy*, 51(9), 1813–1821. <https://doi.org/10.1002/jrs.5670>
- Kim, S. T., O'Neil, J. R., Hillaire-Marcel, C., & Mucci, A. (2007). Oxygen isotope fractionation between synthetic aragonite and water: Influence of temperature and Mg²⁺ concentration. *Geochimica et Cosmochimica Acta*, 71(19), 4704–4715. <https://doi.org/10.1016/j.gca.2007.04.019>
- Kozdon, R., Ushikubo, T., Kita, N. T., Spicuzza, M. J., & Valley, J. W. (2009). Intrastage oxygen isotope variability in the planktonic foraminifer *N. pachyderma*: Real vs. apparent vital effects by ion microprobe. *Chemical Geology*, 258(3–4), 327–337. <https://doi.org/10.1016/j.chemgeo.2008.10.032>
- Kripa, V., Mohamed, K. S., Appukkuttan, K. K., & Velayudhan, T. S. (2007). Production of Akoya pearls from the Southwest coast of India. *Aquaculture*, 262(2–4), 347–354. <https://doi.org/10.1016/j.aquaculture.2006.09.047>
- Kuk-Dzul, J. G., & Díaz-Castañeda, V. (2016). The relationship between mollusks and oxygen concentrations in Todos Santos Bay, Baja California, Mexico. *Journal of Marine Biology*, 2016(1), 1–10. <https://doi.org/10.1155/2016/5757198>
- Latchere, O., Mehn, V., Gaertner-Mazouni, N., Le Moullac, G., Fievet, J., et al. (2018). Influence of water temperature and food on the last stages of cultured pearl mineralization from the black-lip pearl oyster *Pinctada margaritifera*. *PLoS One*, 13(3), e0193863. <https://doi.org/10.1371/journal.pone.0193863>
- Leng, M. J., & Lewis, J. P. (2016). Oxygen isotopes in molluscan shell: Applications in environmental archaeology. *Environmental Archaeology*, 21(3), 295–306. <https://doi.org/10.1179/1749631414Y.0000000048>
- Linzmeier, B. J., Kozdon, R., Peters, S. E., Valley, J. W. (2016). Oxygen isotope variability within growth bands suggests daily depth migration behavior is recorded in *Nautilus* shell aragonite. *PLoS One*, 1–31. <https://doi.org/10.1371/journal.pone.0153890>
- Linzmeier, B. J., Landman, N. H., Peters, S. E., Kozdon, R., Kitajima, K., Valley, J. W. (2018). Ion microprobe stable isotope evidence for ammonite habitat and life mode during early ontogeny. *Paleobiology*, 44(4), 1–25. <https://doi.org/10.1017/pab.2018.21>
- Mackenzie, C. L., Ormondroyd, G. A., Curling, S. F., Ball, R. J., Whiteley, N. M., & Malham, S. K. (2014). Ocean warming, more than acidification, reduces shell strength in a commercial shellfish species during food limitation. *PLoS One*, 9(1). <https://doi.org/10.1371/journal.pone.0086764>
- Marin, F., Le Roy, N., & Marie, B. (2012). The formation and mineralization of mollusk shell. *Frontiers in Bioscience*, 4(1), 1099–1125. <https://doi.org/10.2741/s321>
- Martinez, M., Mangano, M. C., Maricchiolo, G., Genovese, L., Mazzola, A., & Sarà, G. (2018). Measuring the effects of temperature rise on Mediterranean shellfish aquaculture. *Ecological Indicators*, 88, 71–78. <https://doi.org/10.1016/j.ecolind.2018.01.002>
- Milano, S., Nehrke, G., Wanamaker, A. D., Jr., Ballesta-Artero, I., Brey, T., & Schöne, B. R. (2017). The effects of environment on *Arctica islandica* shell formation and architecture. *Biogeosciences*, 14(6), 1577–1591. <https://doi.org/10.5194/bg-14-1577-2017>
- Murphy, A. E., Jakubek, R. S., Steele, A., Fries, M. D., & Glamoclija, M. (2021). Raman spectroscopy provides insight into carbonate rock fabric based on calcite and dolomite crystal orientation. *Journal of Raman Spectroscopy*, 52(6), 1155–1166. <https://doi.org/10.1002/jrs.6097>
- Nehrke, G., & Nouet, J. (2011). Confocal Raman microscope mapping as a tool to describe different mineral and organic phases at high spatial resolution within marine biogenic carbonates: Case study on *Nerita undata* (Gastropoda, Neritopsina). *Biogeosciences*, 8(12), 3761–3769. <https://doi.org/10.5194/bg-8-3761-2011>
- Nehrke, G., Poigner, H., Wilhelms-Dick, D., Brey, T., & Abele, D. (2012). Coexistence of three calcium carbonate polymorphs in the shell of the Antarctic clam *Laternula elliptica*. *Geochemistry, Geophysics, Geosystems*, 13(5). <https://doi.org/10.1029/2011GC003996>
- Nudelman, F. (2015). Nacre biomineralisation: A review on the mechanisms of crystal nucleation. In *Seminars in cell & developmental biology* (Vol. 46, pp. 2–10). Academic Press. <https://doi.org/10.1016/j.semcdb.2015.07.004>
- Olson, I. C., Blonsky, A. Z., Tamura, N., Kunz, M., Pokroy, B., Romao, C. P., et al. (2013). Crystal nucleation and near-epitaxial growth in nacre. *Journal of Structural Biology*, 184(3), 454–463. <https://doi.org/10.1016/j.jsb.2013.10.002>
- Olson, I. C., & Gilbert, P. U. P. A. (2012). Aragonite crystal orientation in mollusk shell nacre may depend on temperature. The angle spread of crystalline aragonite tablets records the water temperature at which nacre was deposited by *Pinctada margaritifera*. *Faraday Discussions*, 159(1), 421–432. <https://doi.org/10.1039/C2FD20047C>

- Olson, I. C., Kozdon, R., Valley, J. W., & Gilbert, P. U. P. A. (2012). Mollusk shell nacre ultrastructure correlates with environmental temperature and pressure. *Journal of the American Chemical Society*, *134*, 7351–7358. <https://doi.org/10.1021/ja210808s>
- Orland, I. J., Kozdon, R., Linzmeier, B., Wycech, J., Sliwinski, M., Kitajima, K., et al. (2015). Enhancing the accuracy of carbonate $\delta^{18}\text{O}$ and $\delta^{13}\text{C}$ measurements by SIMS. In *AGU Fall Meeting Abstracts* (Vol. 2015, p. PP52B-03).
- Pearson, P. N. (2012). Oxygen isotopes in foraminifera: Overview and historical review. *Paleontological Society Papers*, *18*, 1–38. <https://doi.org/10.1017/s108933260002539>
- Pfister, L., Thielen, F., Delouie, E., Valle, N., Lentzen, E., Grave, C., et al. (2018). Freshwater pearl mussels as a stream water stable isotope recorder. *Ecology*, *11*(7), e2007. <https://doi.org/10.1002/eco.2007>
- Ramesh, K., Melzner, F., Griffith, A. W., Gobler, C. J., Rouger, C., Tasdemir, D., & Nehrke, G. (2018). In vivo characterization of bivalve larval shells: A confocal Raman microscopy study. *Journal of the Royal Society Interface*, *15*(141), 20170723. <https://doi.org/10.1098/rsif.2017.0723>
- Rao, K. V., & Rao, K. S. (1974). Pearl oysters. In *The Commercial Molluscs of India* (Vol. 25, pp. 84–105). Central Marine Fisheries Research Institute Bulletin.
- Rousseau, M., & Rollion-Bard, C. (2012). Influence of the depth on the shape and thickness of nacre tablets of *Pinctada margaritifera* pearl oyster, and on oxygen isotopic composition. *Minerals*, *2*(1), 55–64. <https://doi.org/10.3390/min2010055>
- Saruwatari, K., Matsui, T., Mukai, H., Nagasawa, H., & Kogure, T. (2009). Nucleation and growth of aragonite crystals at the growth front of naces in pearl oyster, *Pinctada fucata*. *Biomaterials*, *30*(16), 3028–3034. <https://doi.org/10.1016/j.biomaterials.2009.03.011>
- Soldati, A. L., Jacob, D. E., Wehrmeister, U., Häger, T., & Hofmeister, W. (2008). Micro-Raman spectroscopy of pigments contained in different calcium carbonate polymorphs from freshwater cultured pearls. *Journal of Raman Spectroscopy*, *39*(4), 525–536. <https://doi.org/10.1002/jrs.1873>
- Spero, H. J., Bijma, J., Lea, D. W., & Bemis, B. E. (1997). Effect of seawater carbonate concentration on foraminiferal carbon and oxygen isotopes. *Nature*, *390*(6659), 497–500. <https://doi.org/10.1038/37333>
- Tomaru, Y., Kumatabara, Y., Kawabata, Z., & Nakano, S. (2002). Effect of water temperature and chlorophyll abundance on shell growth of the Japanese pearl oyster, *Pinctada fucata martensii*, in suspended culture at different depths and sites. *Aquaculture Research*, *33*(2), 109–116. <https://doi.org/10.1046/j.1365-2109.2002.00653.x>
- Trofimova, T., Milano, S., Andersson, C., Bonitz, F. G., & Schöne, B. R. (2018). Oxygen isotope composition of *Arctica islandica* aragonite in the context of shell architectural organization: Implications for paleoclimate reconstructions. *Geochemistry, Geophysics, Geosystems*, *19*(2), 453–470. <https://doi.org/10.1002/2017GC007239>
- Tukey, J. W. (1977). *Exploratory data analysis*. Addison-Wesley Publishing Company.
- Urmos, J., Sharma, S. K., & Mackenzie, F. T. (1991). Characterization of some biogenic carbonates with Raman spectroscopy. *American Mineralogist*, *76*(3–4), 641–646.
- Vihtakari, M., Renaud, P. E., Clarke, L. J., Whitehouse, M. J., Hop, H., Carroll, M. L., & Ambrose, W. G., Jr. (2016). Decoding the oxygen isotope signal for seasonal growth patterns in Arctic bivalves. *Palaeogeography, Palaeoclimatology, Palaeoecology*, *446*, 263–283. <https://doi.org/10.1016/j.palaeo.2016.01.008>
- Wang, X.-L., Coble, M. A., Valley, J. W., Shu, X.-J., Kitajima, K., Spicuzza, M. J., Sun, T. (2014). Influence of radiation damage on late Jurassic zircon from southern China: Evidence from in situ measurement of oxygen isotopes, laser Raman, U-Pb ages, and trace elements. *Chemical Geology*, *389*, 122–136. <https://doi.org/10.1016/j.chemgeo.2014.09.013>
- Watkins, J. M., Nielsen, L. C., Ryerson, F. J., & DePaolo, D. J. (2013). The influence of kinetics on the oxygen isotope composition of calcium carbonate. *Earth and Planetary Science Letters*, *375*, 349–360. <https://doi.org/10.1016/j.epsl.2013.05.054>
- Weber, J. N., & Woodhead, P. M. (1972). Temperature dependence of oxygen-18 concentration in reef coral carbonates. *Journal of Geophysical Research*, *77*(3), 463–473. <https://doi.org/10.1029/JC077i003p00463>
- Wycech, J., Kelly, D. C., Kozdon, R., Orland, I., Spero, H. J., & Valley, J. W. (2018). Comparison of $\delta^{18}\text{O}$ analyses on individual planktic foraminifer (*Orbulina universa*) shells by SIMS and gas-source mass spectrometry. *Chemical Geology*, *483*, 119–130. <https://doi.org/10.1016/j.chemgeo.2018.02.028>
- Yoshimura, T., Nakashima, R., Suzuki, A., Tomioka, N., & Kawahata, H. (2010). Oxygen and carbon isotope records of cultured freshwater pearl mussel *Hyriopsis* sp. shell from Lake Kasumigaura, Japan. *Journal of Paleolimnology*, *43*(3), 437–448. <https://doi.org/10.1007/s10933-009-9341-8>
- Zhou, G. T., & Zheng, Y. F. (2003). An experimental study of oxygen isotope fractionation between inorganically precipitated aragonite and water at low temperatures. *Geochimica et Cosmochimica Acta*, *67*(3), 387–399. [https://doi.org/10.1016/S0016-7037\(02\)01140-7](https://doi.org/10.1016/S0016-7037(02)01140-7)